Streamlining Magnetoelectric Magnetic Field Sensor Testing

Jonathan Tan (Northeastern University, Electrical Engineering), *SUNFEST Fellow*

Troy Olsson, ESE

***Abstract* — Magnetoelectric composite magnetic field sensors have recently shown promise for biomedical applications such as magnetoencephalogram, allowing for rapid room temperature neuroimaging. In this work, an AC magnetic field sensor testing structure is presented to easily perform electric, magnetic, and modulation tests on these devices. The testing structure provides a simple way to quickly characterize the performance of the piezoelectric layer, magnetostrictive layer, and the entire device. The design incorporates a wound electromagnet to provide a DC bias field for the magnetoelectric sensors and a PCB RF coil to reduce its volume and to create a detectable AC magnetic field. The design was 3D printed, providing a stable structure to test the devices on. The structure was designed for a modular setup, allowing different parts to be swapped in and out depending on the test performed and for any future components to be implemented. Further modifications to the structure utilizing the modular setup include a linear Hall effect sensor to precisely determine the DC magnetic field and a rail with adjustable permanent magnetics to allow for perpendicular magnetic field biasing of the sensors.**

***Index Terms*— Biomedical microelectromechanical Systems; magnetic sensors; brain-computer interface; magnetoencephalography**

I. Introduction

Increasingly sensitive magnetic field sensors with small form factors have been sought after recently to detect magnetic fields from the human brain (10 fT to 1 pT) [1]. Magnetoencephalography (MEG), is the procedure of sensing and interpreting magnetic fields produced by the brain. By measuring the MEG signals, researchers can better study areas such as consciousness, epilepsy, and movement disorders [2]. Magnetoelectric (ME) sensors featuring multiferroic composites with piezoelectric and magnetostrictive layers have shown to be viable for MEG [3]. Three tests are performed to determine the efficacy of the piezoelectric layer, magnetostrictive layer, and the device as a whole.

Electrical testing verifies that the resonant frequency of the sensor's beam matches the resonant frequency that the sensor was designed for. From the detected peak on a vector network analyzer (VNA) at this frequency, the device is evaluated to determine if it performs well enough to continue testing. The VNA is connected on each side of the sensor and sends power into one side over a range of frequencies. The amount of power detected at the other side of the sensor is measured at each frequency. At specific resonant frequencies, the piezoelectric layer flexes and stretches greatest, causing a voltage differential due to the properties of piezoelectric materials. This voltage differential is detected by the VNA, and because more power is detected at the resonant frequency than at other frequencies, a clear peak is seen indicating the resonant frequencies. Sharp peaks are desired, as more energy can be transferred from the magnetostrictive layer to the piezoelectric layer when detecting magnetic fields. Electrical testing determines the piezoelectric material's efficacy and confirms the resonant frequency of the beam. Once the piezoelectric layer's performance is confirmed, the magnetostrictive layer is tested magnetically.

Magnetic testing determines the responsivity of the magnetostrictive layer by exposing the device to an AC magnetic field swept around the same frequency range as the beam's resonant frequency. Magnetostrictive materials in ME sensors need to be biased with a DC magnetic field to produce the most strain in an AC magnetic field [4]. For this reason, the DC bias field is adjusted in magnetic testing to determine the optimal bias field for the device. Then, the data at each bias field level is compared to see at which DC bias level the beam's response was greatest. This DC field strength is then used to bias the ME sensor in modulation testing.

Lastly, the modulation test considers the device under full operational conditions. A small external RF magnetic field is driven between 1 Hz to 1 kHz, the range of frequencies produced by the human brain, and the sensor is operated at the device's resonant frequency with an AC voltage at one end of the sensor. The optimum DC magnetic field determined from the magnetic testing is used to bias the sensor. From this setup, the small magnetic field can be detected at the output of the device using a spectrum analyzer. The plot produced in the spectrum analyzer shows a peak at the device's resonant frequency and a smaller peak on either side corresponding to the detected external magnetic fields.

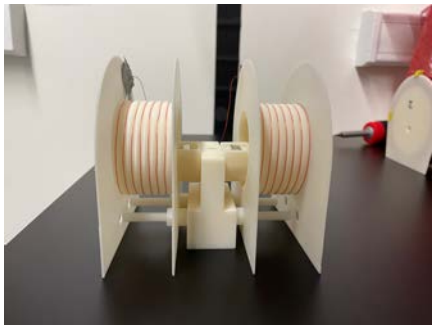

Figure 1: The current structure for testing ME sensors. The center platform holds the sensor. Beside the platform are two permanent magnets for biasing the device, and two RF coils for the device to sense

The current testing setup is shown in Figure 1. This apparatus shows the RF coils on either side of the platform on which the device tested sits. Additionally, two permanent magnets are shown, which are used to bias the devices with a DC bias magnetic field.

In this paper, the design of a new testing structure is explored through an iterative design process, and data from measurements utilizing the apparatus are shown. Stability and ease of use of the testing structure will be explored in its design.

II. Background

A. Magnetoelectric Magnetic Field Sensors

ME sensors operate using two layers: a magnetostrictive layer and a piezoelectric layer. Magnetostrictive materials produce strains and stresses in response to an external magnetic field and piezoelectric materials produce a voltage differential in response to a mechanical strain or stress.

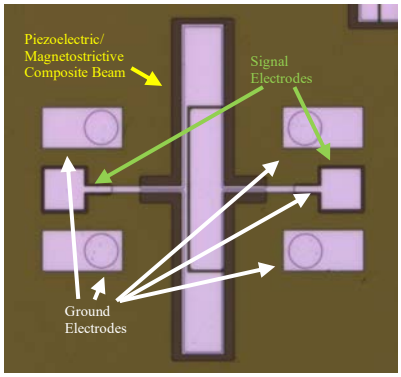

Figure 2: The Design of the Magnetoelectric Magnetic Field Sensors. Four ground electrodes, two signal electrodes, and the magnetoelectric composite beam are shown. The beam resonates, producing a voltage from the piezoelectric layer that is detected at the signal electrode

In ME magnetic field sensors, the magnetostrictive layer is mechanically coupled to the piezoelectric layer, such that any strains or stresses produced in the magnetostrictive layer are transferred to the piezoelectric [3]. The sensors in Figure 2 feature electrodes for ground and signal on either side of the device, a free-floating beam with the piezoelectric and magnetostrictive layers, and tethers holding the beam up to the electrodes.

B. Magnetostriction and Piezoelectricity

Magnetostrictive materials develop a strain when placed in a magnetic field. This is caused by the alignment of the magnetic domains, producing a slight change in the dimensions of the material [5]. The "U" shaped plot of the strain over applied magnetic field plot for magnetostrictive materials in Figure 3 shows that there is an optimal magnetic field at which the greatest change in strain occurs for a small change in magnetic field. For this reason, a DC bias magnetic field is required for ME magnetic field sensors to operate most effectively. To sense magnetic fields from the human brain, the maximum strain in the magnetostrictive layer is desired, as the small brain magnetic fields will cause the most strain that can be coupled to the piezoelectric layer.

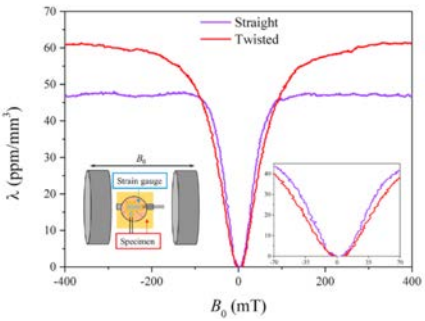

Figure 3: The strain-magnetic field plot. A bias magnetic field is required to produce the most strain per change in magnetic field, shown along the sloped edges of the plot [5]

A piezoelectric material creates a voltage differential across one axis when a strain or stress is applied [6]. On the atomic scale, the crystal structure elongates from a force due to the elasticity of the bonds within the crystal lattice. In the crystal lattice, the charge distribution is asymmetrical in the unit cell, causing a polarization to appear across the unit cell when the crystal structure elongates. Because each unit cell has its own polarization, a net polarization forms, creating a voltage differential when the force is applied to the piezoelectric material [7].

The magnetoelectric magnetic field sensors designed incorporate a thin film beam suspended in air attached to signal electrodes. The beam is made up of the magnetostrictive layer, either an Iron Cobalt (FeCo) or Iron Gallium (Galfenol) alloy, coupled to the piezoelectric layer of Aluminum Nitride (AlN) [5, 8]. The device beam's resonant frequency is found using electrical testing to determine the optimal frequency to drive the piezoelectric material; at this frequency, the strains in the magnetostrictive from the smaller frequency brain magnetic fields are more effectively transferred to the piezoelectric layer. The resonant frequency is a function of properties of the beam such as its dimensions and Young's modulus. When testing the devices electrically, multiple peaks can be seen in the VNA, each corresponding to a different mode of resonance of the beam, such as stretching and bending [3]. The peak of interest is that of the first order extensional mode of the beam, where it stretches and contracts at resonance.

C. Sensors for Magnetoencephalography

Current technologies used for MEG include Superconducting quantum interference devices (SQUIDs) and Optically Pumped Magnetometers (OPMs) [9, 10, 11, 12]. However, SQUIDs require cryogenic temperatures using liquid nitrogen and large machinery to operate. These properties make SQUIDs confined to healthcare facilities with dedicated facilities and readily available liquid helium. OPMs are much smaller, but they require the patient to be tethered to specialized equipment, making the procedure cumbersome.

ME magnetic field sensors are attractive because they address the shortcomings of both SQUIDs and OPMs. ME sensors are able to operate at room temperatures without the need of cryogenic liquids and do not require the patient to be attached to additional external equipment. Because of their ability to work at room temperature without large machinery or tethers to other equipment, ME sensors have the potential to be used in the healthcare industry outside of the hospital for rapid on-site diagnoses.

D. Testing and Measurement Considerations

When testing the sensors electrically, the Q-factor of the piezoelectric layer is an important factor when considering the potential efficacy of the device. The Q-factor for a peak is the frequency of the peak divided by the half power bandwidth (-3dB bandwidth). An example of the output data of electrical testing is in Figure 4, showing the Q factor as well as the resonant frequency and the magnitude of the peak. For peaks with a very sharp peak, the Q-factor is much higher than one with a rounded peak because the half power bandwidth is much larger for a rounded peak. A high Q-factor is desired when

taking electrical measurements because the signal of the carrier and the sidebands are able to be amplified beyond the noise floor. This also explains why the piezoelectric layer is driven at high frequencies in the MHz range; at high frequencies, a high Q-factor means the half power bandwidth encompasses the modulated signal frequencies at $f_{carrier} \pm f_{signal}$. MEG signals frequencies range between 1 Hz and 1 kHz, so the electrical measurement peak should encompass up to 1 kHz from the peak frequency. Based on the equation for the Q-factor, higher peak frequencies result in a wider half power bandwidth for the same Q-factor. Thus, the devices are designed with a high frequency resonant frequency beam in the MHz range; for well performing devices, this allows the half power bandwidth to include frequencies up to 1 kHz from the center peak, amplifying the sideband peaks.

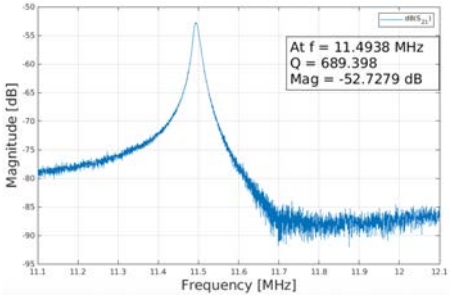

Figure 4: Electrical measurement results. The device beam's resonant frequency is shown to be 11.49 MHz with a Q-factor of 689. This plot shows a desired single-peaked result with a half-power bandwidth encompassing up to 1 kHz

During modulation testing, the external magnetic fields are sensed by the magnetostrictive material, causing a strain that is coupled to the piezoelectric layer. The device acts as a mixer, where the high frequency at which the sensor's beam resonates is modulated by the low frequency of the external magnetic field. When the output of the sensor is detected on the spectrum analyzer, where the magnitude of the signal is plotted for each frequency, the peak of the carrier signal from the device beam's resonant frequency is clearly seen. As shown in Figure 5, on either side of the carrier signal, another peak can be seen, showing the modulated signal (sidebands) of the lower frequencies simulating the frequencies of the human body's magnetic fields. The frequency difference between the modulated signals and the carrier signal is the frequency of the external magnetic field, consistent with the effects of a mixer.

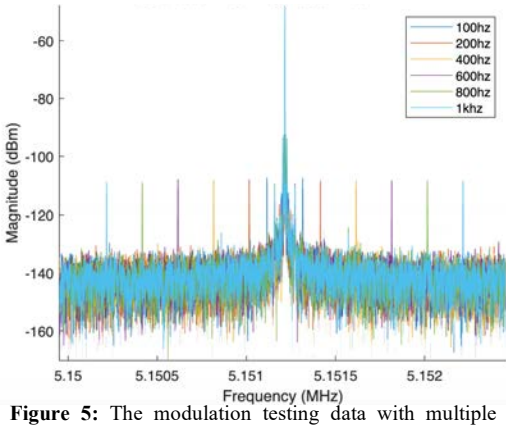

Figure 5: The modulation testing data with multiple magnetic field frequencies plotted on the same figure. Sideband peaks with frequencies of the external magnetic field frequency away from the carrier peak are seen

III. Methods

A. Testing Structure Design

One of the main drawbacks of the current design is that the structure is lightweight and any light force can move the entire object. If the structure was moved during testing, probes or devices could potentially be damaged, which can be costly or time consuming. For this reason, a more stable structure is desired. In the probe station, there is a microscope and stage on which devices can be tested. By designing a cover to fit over the stage, the entire structure would not move if touched. Additionally, the cover could have slots to allow parts to be placed or removed as necessary. This also allows future design iterations of the current components.

Future testing of the devices could use a PCB that connects directly to the device using wire bonds. The PCB trace is then connected directly to SMA connectors. This would provide a package to test the devices instead of using RF probes. Because the width of the PCB is much smaller than that of the RF probes, all components can be moved closer to the device testing platform. For the setup proposed, the stage cover requires two additional sets of notches on either side of the testing platform.

Two magnetic fields are required for magnetic and modulation testing. A DC magnetic field is required for biasing the device and an AC magnetic field to act as the brain's magnetic field. Two options are available for a DC magnetic field: permanent magnets from ferromagnetic materials, or an electromagnet creating a magnetic field following Ampere's Law. When using permanent magnets, the magnets need to be moved along the axis of the device in order to produce varying magnetic field strengths. However, moving the magnets can be imprecise, given that the magnetic field along the axis drops off by the inverse cube of distance; when the magnets are close to the device, the magnetic field changes drastically for a small movement of the magnets. Another option is an electromagnet, which consists of a wound wire coil with a current passing through the wire. This results in a magnetic field perpendicular to the coil of wire with a strength linearly dependent on the current. However, electromagnets can only produce small magnetic field strengths without many turns of the coil or a large current.

In this application, a precisely configurable magnetic field is desired to precisely bias a device for its optimal performance. For this reason, an electromagnet was pursued to provide a DC magnetic field for biasing the ME magnetic field sensors, as the current controllable magnetic field is more precise than moving permanent magnets. To produce the most magnetic field, the maximum current through the coil is desired. The power supply can only provide 5 A for up to 6 V, meaning the two electromagnets in series can only be a total of 1.2 Ω in total. Previous electromagnets wound in the lab used 17 AWG wire; using a thicker wire such as 14 AWG would provide a lower resistance per length. This would allow more turns of the coil to reach 1.2 Ω compared to the 17 AWG wire.

The magnetic field produced at the location of the device can be modeled using the following equation [13]

$$B_Z = \frac{\mu_0}{2} In \left(\frac{a}{\sqrt{R^2 + a^2}} + \frac{L - a}{\sqrt{R^2 + (L - a)^2}} \right)$$

where *I* is the current through the wire, *n* is the number of turns in the coil, *a* is location along the z axis from the edge of the coil, *R* is the radius of the coil, and *L* is the length of the coil. From this equation, the parameters for the length and radius of the coil can be adjusted to produce the most amount of DC magnetic field at the location of the device. This equation also verifies that the magnetic field at a location *a* is linearly dependent on the amount of current through the wire. This shows that the amount of magnetic field produced at the device

location can be easily tuned by increasing or decreasing the current through the electromagnet.

To create an AC magnetic field, a similar coil like the DC coil is needed. However, instead of using a wound coil like the one currently used, a printed circuit board (PCB) was created to reduce the size occupied by the RF coils. This grants the space to use electromagnets, as using wound coils for both electromagnets and RF coils would not fit on the microscope stage. The PCB coils were designed on Autodesk Eagle, and the Texas Instruments Webench Coil Designer [14] and Coil32 [15] were used to choose parameters of the coil such as trace width and inner and outer radii. Two designs of the coils were created, one with a coil on only one layer and another with coils on either side of the PCB. The single layered design is shown in Figure 6. For the final design, it was determined that the coil should have an outer diameter of about 9 cm to fit in the microscope setup, 2 turns of the coil, and an inner diameter of about 8.5. These parameters allow the coil to stay inductive up to 25 MHz without a large inductance. Above a cutoff frequency, RF coils become more capacitive than inductive, producing undesirable losses due to electric fields produced between coil windings. The cutoff frequency specifies the frequency at which the coils become capacitive. However, the coils should not have a large inductance. Because the coils are operated at the megahertz range, a large inductance will result in a large impedance. This results in the coil acting as an open circuit. An open circuit prevents any current from running through, resulting in no magnetic field being produced. To fit onto the stage cover, the PCB coils were attached with a plastic rivet to a plastic plate that could be fit onto the stage cover.

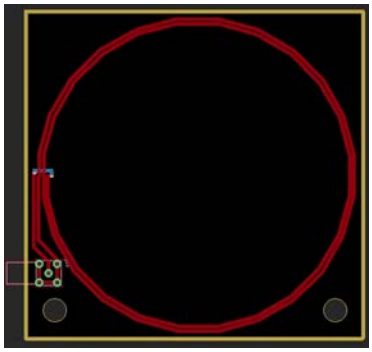

Figure 6: The single layered PCB RF coil used at low frequencies to mimic the brain in modulation testing and at high frequencies to drive the device in magnetic testing

The current method of detecting the DC magnetic field bias is by using a DC magnetic field probe and testing the magnetic field at specific distances for the permanent magnets. A method of measuring the DC magnetic field during testing is desired, reducing the amount of uncertainty and any error in the magnetic field bias. To accomplish this, a Hall effect sensor was used to measure the magnetic field bias during testing. By connecting 5 volts and ground to the sensor, the output of the device can be connected to a multimeter. The output voltage changes linearly with the amount of magnetic field present through the device. This device can be used during testing to precisely measure the amount of bias field the magnetostrictive layer optimally operates at. A drawer in the device testing platform was created, in which the Hall effect sensor is located and measures the magnetic field.

In some cases, the magnetic field sensors are tested with a perpendicular magnetic field bias. In a perpendicular bias, the amount of magnetic field required to bias the device is much higher than parallelly. For this reason, permanent magnets are the ideal option to perpendicularly bias the devices. The permanent magnets are smaller and can reach larger magnetic fields than electromagnets. Inspiration was taken from the current design to create the perpendicular bias magnet setup. Magnets were placed on rails such that the magnets can be moved closer to or farther from the device, increasing and decreasing the magnetic field bias through the device respectively. The rail was run through the device testing platform. The magnet 'buckets' were created such that the magnetic field bias through the device is horizontal. This required the buckets to be high enough to be on the same level with the device. However, the buckets had to be low enough to not interfere with the RF probes directly above the magnets. Lastly, lids were created for each of the buckets to prevent the magnets from jumping out of the buckets. Because the distances are small between the two magnets, they could potentially jump out from magnetic forces and collide with the devices or RF probes.

B. Electrical, Magnetic, Modulation Testing

Three tests are used to test the performance of the materials and devices. Electrical testing determines the efficacy of the piezoelectric layer of the device and confirms the resonant frequency of the resonating beam. Magnetic testing determines the optimal DC magnetic field bias and how well the magnetostrictive layer performs. Modulation testing takes the entire device into consideration, seeing how the device performs in detecting small external magnetic fields.

In electrical testing, power is driven into one end of the device and detected at the other end using the S21 measurement of the VNA. The ratio of power detected to power delivered is plotted over a sweep of frequencies and shows a peak at the resonant frequency of the device's beam. The frequency of the peak is measured and compared to the frequency that it is designed to have, confirming the resonant frequency of the beam. As previously mentioned, a large Q-factor for the resonance peak is desired because the output power of the device is amplified by the Q-factor

Magnetic testing drives the devices magnetically to determine the functionality of the magnetostrictive layer and find the optimum magnetic field bias for the device. Power is supplied to RF coils operating in a sweep of frequencies around the resonant frequency determined in electrical testing, and the amount of power detected at one end of the device is measured. In the plot of the ratio between the power detected to power supplied over a sweep of frequencies, a peak close to the noise floor can be seen. Because the magnetic fields produced by the RF coils are small, little power is delivered to the magnetostrictive layer to resonate the beam. This means less power is transformed into a voltage by the piezoelectric, resulting in an output peak close to the noise floor.

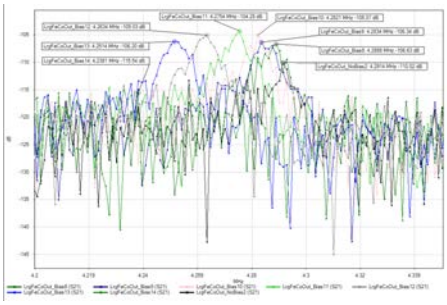

Figure 7: Magnetic testing with multiple trials of varying bias field strengths on one plot. The peaks shift due to the ΔE effect

Multiple magnetic tests are performed for a device, each at a different magnetic field bias. When the data from these tests are

plotted on one figure, multiple peaks are shown. Each peak is shifted slightly in frequency due to the ΔE effect; as more magnetic field bias is applied, the magnetostrictive layer slightly lengthens. Because the resonant frequency of the beam is a function of the length, width, and other parameters, the resonant frequency of the beam decreases in a larger magnetic field bias. The figure with multiple data plots is also used to determine the optimal magnetic field bias by finding the largest peak of the different plots. A plot with multiple data sets of varying magnetic field bias is in Figure 7. The optimal magnetic field bias along the stress-magnetic field plot provides the largest change in strain for a small AC magnetic field, producing the largest peak in the magnetic testing results.

Modulation testing drives the device electrically and magnetically to determine how well it can measure small AC magnetic fields. The magnetostrictive layer is biased with a DC magnetic field, the piezoelectric layer is driven at one end of the device with an AC voltage at the beam's resonant frequency, and the RF coils are driven between 1 Hz and 1 kHz to mimic the brain. The output of the device is sensed with a spectrum analyzer, showing the power at the output of the device over a range of frequencies. The device acts as a mixer, multiplying the AC resonant frequency signal with the small frequency signal from the magnetic field, producing a plot with a large carrier signal at the resonant frequency and two sideband modulated signals with peaks that are the small magnetic field's frequency from the carrier signal. Multiple plots testing the device at different AC external magnetic fields can be overlaid onto each other, producing a plot with a carrier signal and multiple sideband peaks. This is used to make sure the device is not attenuating the larger frequency signals at 1 kHz.

IV. Experimental Results and Discussion

A. Testing Structure Results

The testing structure was fabricated by 3D printing each component, winding the DC coils, wiring the Hall effect sensor circuit, and manufacturing the PCB RF coils. Two iterations of the microscope stage cover and DC coils were produced, whereas the other components were only created once.

The 3D printed test structure was printed in two iterations with the microscope stage cover 3D printed twice. The first print was primarily used to determine how much the 3D prints would shrink during printing. Once the first stage cover was received, it was determined that there was minimal shrinkage in the prints. This stage cover was not suitable for using in the final design however. Because the file used the measured dimensions of the microscope stage, there was enough uncertainty in the dimensions that the stage cover did not fit. While the plastic could have been sanded to fit, it was determined that the dimensions should be made larger to prevent any chances of damaging the stage while trying to fit the cover on. Additionally, the first iteration was printed without the two sets of notches to accommodate the wire bonded PCB with SMA connectors. The second iteration of the stage cover took both ideas into consideration. Each dimension of the stage cover was increased by 4% to fit onto the microscope stage, and additional notches were placed 1 cm closer to the device platform.

The DC magnetic field coils were also fabricated twice. The first coil featured an inner radius of 2.5 cm and an outer radius of 4.5 cm. With these dimensions, only 150 turns of 14 AWG wire were able to be wound. Rather than being limited by the power supply output, the coil was constrained by the number of turns, as the resistance of the coil was only 0.463Ω for the turns that could fit in the 4.5 cm radius. This meant more turns could be achieved to reach the 0.6Ω needed before the magnetic field is constrained by the power supply. This first iteration was able to produce up to 2.9 mT at the device location and up to 9.6 mT at the edge of the coil. By adding a magnet in the center of the coil, the magnetic field could be increased; the magnet not only adds its own magnetic field to that produced by the coils, but the ferrite magnet's permeability is higher than that of air, allowing larger magnetic fields to be formed within the magnet than could be created in air. With the magnet added to the core of the coil, up to 6 mT could be measured at the device testing location and up to 25 mT at the edge of the coil.

To improve off the first design, the inner radius was decreased to allow for more turns of the coil. The outer radius was kept the same because increasing the outer radius would elevate the center of the coil above the location of the device testing platform, resulting in magnetic fields at the device that are angled and not parallel to the device surface. With a smaller inner radius, 240 turns were able to be achieved, resulting in up to 9.5 mT at the device location without a magnet and up to 13.5 mT with a magnet. At the edge of the coil, the magnetic field was measured to be 12.4 mT without a magnet and 22.9 mT with a magnet in the core. The resistance of a single coil was found to be 0.58Ω, which is still not optimized for the power supply but better optimized than the first iteration.

The RF coils were fabricated, and its impedance and AC magnetic field amplitude were determined. For RF coils, inductive coils are desired, as the power through the coil is transformed into a magnetic field instead of capacitive losses. These losses can occur because the space between coil turns is insulating, and a capacitance can appear between turns of the wire. This turns the power supplied to the coil into an electric field instead of the desired magnetic fields.

The characterizations of the single and double layered RF PCB coils are below in Figure 8. The Smith chart shown displays the real and imaginary components of the impedance of the coil across a span of frequencies. Above the middle horizontal axis, the coil is inductive, and below the horizontal axis, the coil demonstrates capacitive losses. Lines in the upper half are desired, as it indicates that the coils are inductive. In this plot, it is shown that the single layered PCB stays inductive up to 20 MHz, while the double layered PCB becomes capacitive around 14.8 MHz. The AC magnetic field amplitude of the coils were determined to be 20 μT for the

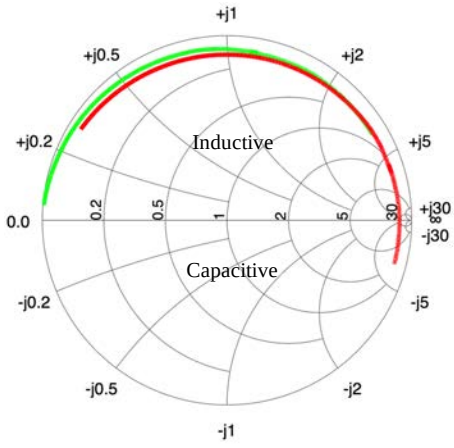

Figure 8: Smith chart of the single layer (green) and double layer (red) PCB coils from 1 MHz to 20 MHz. The double layered PCB coils become capacitive at a lower frequency than the single layered coils

single layered PCBs, which is large enough for the devices to detect and measure during modulation testing and drive the devices in magnetic testing.

The perpendicular bias magnets components were 3D printed, and magnets were placed inside the 'buckets'. The maximum magnetic field bias with the perpendicular bias magnets was 8.6 mT. The magnetic field strengths measured suffice for the large magnetic fields required for perpendicular biasing.

Lastly, the Hall effect sensor circuit was wired, and the sensor was placed into the drawer that was 3D printed for the circuit. The DRV5055A2QLPGM by Texas Instruments was chosen because it is a linear Hall effect sensor that can detect magnetic fields with a $\pm$42 mT range and operates with a 5 V source. By connecting the V_{CC} pin to 5 volts, the GND pin to ground, and the OUT pin to a multimeter set to measure DC voltages, the magnetic field strength in mT can be measured by dividing the difference between the voltage reading and 2.5 V by 50 mV. This provides a method of directly measuring the DC bias field through the devices during testing instead of measuring the magnetic field bias before testing and using the previous values to approximate the bias field through the devices during testing.

B. Testing Results

The testing setup was used for electrical, magnetic, and modulation testing. While the structure was not strictly necessary for electrical testing, as the only test equipment needed was the RF probes and the VNA, testing on the structure provided an easy transition between electrical and magnetic testing, as very little additional setup was required to transition between tests.

A medium FeCo In device was tested electrically on the designed structure. The peak is seen at 9.5 MHz, and the testing structure provided a solid platform to test the device on.

Next, the device was tested magnetically. The VNA was connected to both RF PCB coils using an SMA T connector to connect both PCBS to the same VNA port, the other port of the VNA was connected to one RF probe at one end of the device. On the other end of the device, the RF probe was attached with a ground cap, connecting the signal electrode to ground for better signal stabilization. The Hall effect sensor was connected to 5 V, ground, and the DC voltmeter. The electromagnets were connected in series to provide 5 A through each coil, and the coils were connected to a 6 V, 5 A power supply. The magnetic testing data were measured for varying magnetic bias fields, and the results were shown on a single plot in Figure 9. In this figure, it shows that the largest amplitude signal is at no bias field. This is likely due to the devices being tested with no bias field after testing them at a higher magnetic field bias. Because the magnetic dipoles in the magnetostrictive layer do not immediately return to random after a magnetic field bias is removed, the dipoles may keep their rotation and stay biased despite no magnetic field through the material. This would explain why the 0 field level bias presented the highest amplitude. The device was first tested at a high magnetic field bias, and the device likely kept its bias when the electromagnets were disconnected.

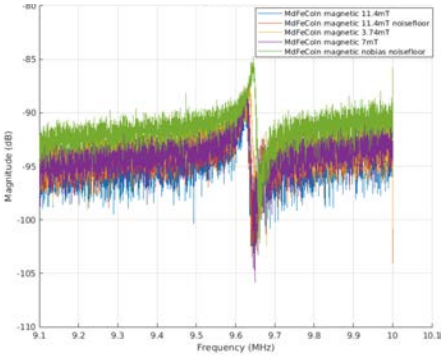

Figure 9: Magnetic testing plots at different bias fields on one figure. The measurements were performed on the designed testing structure

Lastly, a modulation test was performed on the devices. The results of the modulation tests with an external magnetic field at 200, 400, 600, and 800 Hz are shown in Figure 10. The device is able to detect the low magnetic fields produced by the PCB coils. However, the signal to noise ratio is lower at 17 compared to previous modulation tests with SNR of around 30. This could be due to a few factors. First, the PCB coils have fewer turns than the wound RF coils. Because there are fewer turns, the magnetic field strength of the PCBs could be lower than that produced by the wound coils. However, the magnetic field strength of the wound coils was also measured to be around 20 μT, similar to that of the PCB coils. Additionally, the RF coils could be coupling to the DC coils, resulting in lower magnetic field strengths than expected at the device location and a lower SNR as a result.

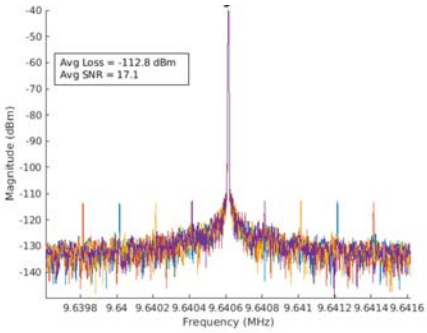

Figure 10: The results of multiple modulation tests at varying magnetic field frequencies tested on the designed structure

V. Conclusion

In this work, a magnetoelectric magnetic field sensor setup was designed and constructed. The structure was designed to easily test the magnetic field sensors electrically, magnetically, and with a modulation test. Components in the structure were 3D printed, with additional parts added on, including electromagnets and a circuit for a Hall effect sensor. The structure was designed to be modular, so future components can be easily integrated into the testing structure. Compared to the current testing setup, the constructed structure is more stable because of the microscope stage cover that prevents movement and allows for components to be securely fit into notches. The DC electromagnets provide a current tunable magnetic field up to 13.5 mT that can be precisely controlled compared to the previous permanent magnets, and the PCB RF coil volume is much smaller than that of the wound RF coils while producing comparable magnetic field strengths. The constructed design additionally allows the user to precisely measure the magnetic field bias through the device using the Hall effect sensor during testing. These improvements to the previous design create a testing structure that can be easily used for performing electrical, magnetic, and modulation testing, easing the process of characterizing these devices.

ACKNOWLEDGEMENT

The author acknowledges Dr. Troy Olsson, Sydney Sofronici and Michael D'Agati, and the entire Olsson group of the University of Pennsylvania for an incredible research experience this summer, the National Science Foundation for funding the SUNFEST program with NSF REU grant no. 1950720, Dr. Sue-Ann Bidstrup Allen and Julia Falcon of the University of Pennsylvania for organizing the SUNFEST REU, and the University of Pennsylvania Libraries' Biomedical Library for 3D printing the structure components.

REFERENCES

[1] M. HÄMÄLÄINEN et al, "Magnetoencephalography—theory, instrumentation, and applications to noninvasive studies of the working human brain," Reviews of Modern Physics, vol. 65, (2), pp. 413-497, 1993. Available: https://explore.openaire.eu/search/publication?articleId=dedup_wf_001::27c2bf09e0a170aa7b5d02de6c9a8018. DOI: 10.1103/RevModPhys.65.413.

[2] S. Baillet, "Magnetoencephalography for brain electrophysiology and imaging," Nature Neuroscience, vol. 20, (3), pp. 327-339, 2017. Available: https://www.ncbi.nlm.nih.gov/pubmed/28230841. DOI: 10.1038/nn.4504.

[3] R. Jahns et al, "Giant Magnetoelectric Effect in Thin-Film Composites," Journal of the American Ceramic Society, vol. 96, (6), pp. 1673-1681, 2013. Available: https://api.istex.fr/ark:/67375/WNG-6NS5WS00-P/fulltext.pdf. DOI: 10.1111/jace.12400.

[4] J. Zhai et al, "Giant magnetoelectric effect in Metglas/ polyvinylidene-fluoride laminates," Appl. Phys. Lett, vol. 89, 2006.

[5] Z. Yang et al, "Structural design and performance evaluation of FeCo/epoxy magnetostrictive composites," Composites Sci. Technol., vol. 210, pp. 108840, 2021. Available: https://www.sciencedirect.com/science/article/pii/S0266353821001962. DOI: https://doi.org/10.1016/j.compscitech.2021.108840.

[6] J. Yang, An Introduction to the Theory of Piezoelectricity. (2nd ed. 2018 ed.) 20189Available: http://cds.cern.ch/record/2653133. DOI: 10.1007/978-3-030-03137-4.

[7] D. Damjanovic, "Piezoelectricity," in Encyclopedia of Condensed Matter Physics, F. Bassani, G. L. Liedl and P. Wyder, Eds. Oxford: Elsevier, 2005, pp. 300-309.

[8] F. Martin et al, "AlN1," Journal of Vacuum Science & Technology A, vol. 22, 2004.

[9] R. Körber et al, "SQUIDs in biomagnetism: a roadmap towards improved healthcare," Supercond. Sci. Technol., vol. 29, (11), 2016. . DOI: 10.1088/0953-2048/29/11/113001.

[10] E. H. Brandt, "Thin superconductors and SQUIDs in perpendicular magnetic field," Physical Review. B, Condensed Matter and Materials Physics, vol. 72, (2), 2005. Available: https://arxiv.org/abs/cond-mat/0506144. DOI: 10.1103/PhysRevB.72.024529.

[11] E. Boto et al, "Moving magnetoencephalography towards real-world applications with a wearable system," Nature, vol. 555, (7698), pp. 657, 2018. . DOI: 10.1038/nature26147.

[12] T. M. Tierney et al, "Optically pumped magnetometers: From quantum origins to multi-channel magnetoencephalography," NeuroImage (Orlando, Fla.), vol. 199, pp. 598-608, 2019. Available: https://dx.doi.org/10.1016/j.neuroimage.2019.05.063. DOI: 10.1016/j.neuroimage.2019.05.063.

[13] P. Grundpraktikum, "E 7e "Magnetic Fields in Coils" Tasks,"

[14] Texas Instruments, "Coil Designer," *Coil designer*, 2014. [Online]. Available: https://webench.ti.com/wb5/LDC/#/spirals. [Accessed: 06-Aug-2021].

[15] Coil 32, "Ferrite toroid calculator," *Coil32*, 30-Mar-2015. [Online]. Available: https://coil32.net/pcb-coil.html. [Accessed: 06-Aug-2021].